On the Active Role of Temperature in Surface-Layer Turbulence

GABRIEL G. KATUL AND MARC B. PARLANGE*

Hydrologic Science, Department of Land, Air, and Water Resources, University of California, Davis, California

(Manuscript received 18 November 1992, in final form 30 April 1993)

ABSTRACT

Orthonormal wavelet expansions were derived and applied to atmospheric surface-layer turbulence measurements of temperature and vapor concentration under unstable and stable atmospheric stability conditions. These expansions were used to investigate both the statistical and spectral structure of turbulence simultaneously in space and scale using two tracers: temperature and specific humidity. It was found that at small wavenumbers, both temperature and specific humidity Fourier and wavelet spectra exhibit a -1 power law behavior consistent with other atmospheric boundary-layer experiments. The mean values of the energy spectrum obtained from the wavelet analysis are in agreement with the classical Fourier counterparts. The wavelet flatness factors (values up to 10) indicate strong deviation from Gaussian statistics in space for the temperature fluctuations as the wavenumber increases. In contrast, the spatial wavelet flatness factor for the specific humidity exhibits near Gaussian statistics (values up to 4) for all wavenumbers. The wavelet skewness in space indicates that the specific humidity attains a near-isotropic state with increasing wavenumber for both stability conditions. Unlike the specific humidity, the temperature wavelet skewness in space did not decay with increasing wavenumber, indicating the presence of large eddy anisotropy in space. Land surface heating/cooling inhomogeneity appears to affect the local structure of turbulence, and therefore, at small scales temperature behaves as an active scalar when compared to specific humidity. The active role of temperature was also analyzed within the framework of Bolgiano's spectral theory. Deviations from Bolgiano's theory for the temperature spectrum were observed at all wavenumbers with measured energy power law behavior of $|1.2|$, which is less than the theoretical value of $|7/5|$. Conditional wavelet analysis was developed and used to investigate the nature of these deviations from Bolgiano's scaling law for the temperature measurements. It was found that by suppressing energy-containing and intermittent events, Bolgiano's scaling law for the temperature spectrum held under stable stability conditions. The effect of different wavelet basis functions on the statistical and spectral description of atmospheric turbulence was also considered.

1. Introduction

Transport mechanisms in the atmospheric surface layer responsible for the removal of water vapor and heat close to the ground surface are strongly influenced by the large-scale eddy motion. In a recent study, Kader and Yaglom (1991) suggested that the large-scale turbulence spectrum should scale with variables that affect the mean flow (see also Tennekes and Lumley 1972, p. 264) and are given by

$$\frac{E_i(k)}{zu_*^2} = F_i\left(kz, \frac{z}{L}\right)$$

$$\frac{E_T(k)}{zT_*^2} = F_T\left(kz, \frac{z}{L}\right)$$

$$\frac{E_q(k)}{zq_*^2} = F_q\left(kz, \frac{z}{L}\right), \qquad (1)$$

where k is the wavenumber, E_i is the spectrum of velocity components u_i (u_1 is the longitudinal velocity fluctuation along the mean horizontal wind speed U, u_2 is the lateral velocity fluctuation, and u_3 is the vertical velocity fluctuation), E_T is the temperature fluctuation spectrum, E_q is the specific humidity spectrum, z is the height above the ground surface, $u_* = (-\langle u_1 u_3\rangle)^{1/2}$ is the friction velocity, $T_* = (\langle u_3 T\rangle / u_*)$, $q_* = (\langle u_3 q\rangle / u_*)$, $L = -u_*^3/[(k_v g/T_a)\langle u_3 T\rangle]$ is the Obukhov length, $k_v = 0.4$ is von Kármán's constant, g is the gravitational acceleration, q is the specific humidity fluctuation, T is the temperature fluctuation, T_a is the mean temperature of the surface layer, and $\langle\cdot\rangle$ is the averaging operator.

One of the main difficulties with the application of Fourier transforms to study the statistical and spectral properties of large-scale turbulence simultaneously in

* Also affiliated with the Department of Biological and Agricultural Engineering, University of California, Davis.

Corresponding author address: Dr. Marc B. Parlange, Hydrologic Science Division, Department of Land, Air and Water Resources, University of California, Davis, CA 95616.

space and scale is the global nature of the Fourier transform in which spatial information becomes implicit in the phase angle. A flow decomposition is required in which contributions from different scales, as well as different locations, are explicit. Hence, it is preferable to employ kernels that operate as localized pulses rather than extended waves. Conditions of self-similarity of these kernels yield special functions called "wavelets" that are generated by translation and dilation of a single function (Grossmann et al. 1989). Wavelet transforms are recent mathematical tools based on group theory of square integrable functions that allow decomposition of signals, functions, or operators into space and scale. Continuous wavelet transforms were introduced by Grossmann and Morlet (1984, 1985) and have been applied to turbulence by many investigators (e.g., Farge 1992a,b; Everson et al. 1990; Argoul et al. 1989; Liandrat and Moret-Bailly 1990). It should be pointed out that Lumley's eddy, which is associated with many Fourier modes and the phase relation among them, has the desired property of being compact in physical space as well as wave space and can be considered to be a continuous wavelet (Tennekes and Lumley 1972, p. 259). Discrete wavelet transforms constructed from orthonormal wavelets are now being developed and applied to turbulence (Daubechies 1988; Mallat 1989a,b; Meneveau 1991a,b; Mahrt 1991). The orthonormal wavelet expansion method differs from the continuous case in that it forms a complete orthonormal basis, while the continuous wavelet transform forms an overcomplete basis, which can bring about undesired relationships between the wavelet coefficients (Yamada and Ohkitani 1990, 1991a,b; Meneveau 1991a; Kumar and Foufoula-Georgiou 1993). Orthonormal wavelet expansions conserve signal information; that is, a discretely sampled turbulent signal at N points yields N wavelet coefficients, while in the continuous case, the transform can yield up to N^2 coefficients. Note that the orthonormal wavelet expansion is different from the method of "proper orthogonal decomposition" (POD) used by Lumley (1970). POD, also known as the Karhunen–Loeve expansion, is a procedure for decomposing a stochastic field in an L^2 optimal sense. The POD allows the construction of basis functions that maximize the amount of turbulent energy contained in a minimum number of modes in the average sense (Berkooz 1992; Lumley 1981, 1970, p. 57). In contrast, orthonormal wavelet decomposition does not optimize or minimize the number of modes, so that the number of wavelet coefficients needed for turbulence analysis is very large. However, this large number of wavelet coefficients is essential to obtain reliable spatial statistics of instantaneous realizations of turbulent flows.

In this study, we make use of orthonormal wavelet transformations to analyze the structure of turbulence in space and scale close to the land surface. Rapid measurements of temperature and specific humidity are collected at 80 cm over a uniform and dry bare soil surface under different atmospheric stability conditions. The similarity in spatial statistics of the temperature and vapor transport at production as well as near production wavenumbers is investigated. We note that close to the ground surface, large inhomogeneity in heating or cooling of the ground surface may significantly influence the turbulence transport mechanisms of heat (Kader and Yaglom 1990). Since the soil surface was relatively dry, the inhomogeneity in the specific humidity at the ground surface was much smaller than the temperature variation. Statistical tools are used in this similarity investigation since they do not depend on any specific model underlying the structure of turbulence or energy cascading. Within this framework, "dual spectra" proposed by Meneveau (1991a,b) are used for both measured temperature and specific humidity measurements. Dual spectra are wavelet spectra in which an estimate of the mean as well as the spatial standard deviation of the energy at different wavenumbers can be quantified. The localization in physical space amplifies time or space differences in the wavelet transformed measurements so that rapid changes (such as sharp edges of main events) are magnified at different scales. Therefore, statistical measures such as wavelet skewness and flatness factors of the wavelet transformed measurements, at a certain scale, are strongly affected by the horizontal gradients in the original signal. These statistical measures are to detect the similarity/dissimilarity between temperature and specific humidity fluctuations. We also investigate the influence of the wavelet basis function on the spatial and spectral statistics of atmospheric turbulence.

2. Wavelet transforms

Wavelet transforms have become popular since they allow the decomposition of data, functions, or operators into different frequency or scale components. Each component can then be studied with a resolution that matches its scales (i.e., at high frequency the wavelet is very narrow, while at low frequency the wavelet is broad). As a result, wavelet transforms are better capable, compared to windowed Fourier transforms, to "zoom in" on short-lived high-frequency phenomena, such as transients or singularities in signals (see Daubechies 1992, chapter 1). There are many types of wavelet transforms, and for the purpose of this study they are classified under two broad categories: (i) continuous wavelet transforms and (ii) discrete wavelet transforms (Chui 1992; 13–22). Daubechies (1992, p. 7) further classified the discrete wavelet transforms as (i) redundant discrete systems (also known as frames) and (ii) orthonormal wavelet expansions. For actual turbulence measurements of some turbulence flow property $f(x)$, discrete wavelet transforms are desired since $f(x)$ is generally known at only discrete points x_j depending on the resolution of the sensor and the sam-

pling frequency. Also, as shown by Yamada and Ohkitani (1990, 1991a,b), orthonormal wavelet transforms are preferable since the orthogonality condition can suppress undesired relations between the wavelet coefficients. Therefore, it is necessary to discretize the scale and space domain to conserve the amount of information in the signal (Daubechies 1988). As shown by Daubechies (1988, 1992, p. 10) and Mallat (1989a,b), a logarithmic uniform spacing for the scale discretization with increasingly coarser spatial resolution at larger scales allows a complete orthogonal wavelet basis to be constructed. These basis functions are defined by

$$\psi_{[j]}^{(m)}(y) = a_0^{-m/2}\psi\left(\frac{y - jb_0a_0^m}{a_0^m}\right), \qquad (2)$$

where m and j are variable scale and position indexes, respectively, a_0 is the base of the dilation, and b_0 is the translation length in units of a_0^m. The simplest and most efficient case for practical computations is the dyadic arrangement resulting in $a_0 = 2$ and $b_0 = 1$ (Daubechies 1992, p. 10; Chui 1992, p. 4). All scales along octaves 2^m and translations along $2^m j$ contribute to the construction of $f(x_j) = f(j)$ using

$$f(j) = \sum_{m=1}^{m=\infty}\sum_{i=-\infty}^{i=+\infty} W^{(m)}[i]g^{(m)}[i - 2^m j], \qquad (3)$$

where $g^{(m)}[i]$ is a discrete version of the continuous wavelet $\psi(x)$ at scale m. Details regarding the discretization of continuous wavelets $\psi(x)$ are discussed in section 2a. The discrete function $g^{(m)}[i]$ satisfies the orthogonality condition

$$\sum_{k=-\infty}^{k=+\infty} g^{(m)}[k - 2^m j]g^{(n)}[k - 2^n j] = \delta_{ij}\delta_{mn}, \qquad (4)$$

where δ_{ij} is the Kronecker delta. The discrete wavelet coefficients at scale index m and position index i can be obtained by the following convolution,

$$W^{(m)}[i] = \sum_{i=-\infty}^{i=+\infty} g^{(m)}[i - 2^m j]f(j), \qquad (5)$$

and they satisfy the conservation of energy condition

$$\sum_{j=-\infty}^{+\infty} f(j)^2 = \sum_{m=1}^{m=+\infty}\sum_{i=-\infty}^{i=+\infty} (W^{(m)}[i])^2, \qquad (6)$$

which is similar to Parseval's identity in Fourier series (Chui 1992, p. 12).

In general, the number of observations are finite and the summations in the above equations do not extend to infinity. If $N = 2^M$ is the number of observations (i.e., N is an integer power of 2), the scale index m then varies from 1 to $M = \log_2(N)$ and the position index at scale m varies from 1 to $N \times 2^{-m}$. Note that as the scale increases, the spatial resolution becomes much coarser (e.g., at $m = 1$, we have $N/2$ coefficients, at $m = 2$ we have $N/4$ coefficients, at $m = M$ we have 1 coefficient). Note also that the above arrangement conserves the number of wavelet coefficients ($=N - 1$) required to decompose a signal defined over N points. Finally, this dyadic arrangement is suitable for turbulence studies since the small-scale features of the turbulent flow, which can change rapidly compared to the large-scale features, are characterized by more wavelet coefficients.

a. Multiresolution analysis

In this section, multiresolution analysis as developed by Mallat (1989a,b) is briefly discussed. This review is intended to illustrate how both $g^{(m)}[i]$ is obtained from the continuous wavelet $\psi(x)$ and how the computation of the discrete wavelet coefficients is carried out.

In general, turbulence measuring devices can only sample a continuous process $f(x)$ at finite resolution (assumed unity for normalization purposes). Following Meneveau (1992a) and Kumar and Foufoula-Georgiou (1993), it can be shown that there exists a set of orthonormal basis functions $\phi^{(0)}(x - i)$ that, by translation only, generate $f(x)$ using

$$f(x) = \sum_{i=-\infty}^{i=+\infty} s^{(0)}[i]\phi^{(0)}(x - i)dx, \qquad (7)$$

where $s^{(m=0)}[i]$ is given by the convolution

$$s^{(m=0)}[i] = \int_{-\infty}^{+\infty} f(x)\phi(x - i)dx. \qquad (8)$$

In practice $\phi(x)$ is selected to have a fast decay away from the origin and satisfies the orthonormality condition

$$\int_{-\infty}^{+\infty} \phi^{(0)}(x - i)\phi^{(0)}(x - j)dx = \delta_{ij} \qquad (9)$$

so that $s^{(m=0)}[i]$ represents discrete samples of $f(x)$ at unit resolution ($m = 0$) on a mesh i of unit size. Consider $f(x)$ at coarser resolution $R_m = 2^m$ denoted by $f^{(m)}(x)$ [which can be completely extracted from $f(x)$]. Analogous to (7), $f^{(m)}(x)$ is computed from the convolution

$$f^{(m)}(x) = \sum_{i=-\infty}^{i=+\infty} s^{(m)}[i]\phi^{(m)}(x - 2^m i), \qquad (10)$$

where $s^{(m)}[i]$ is given by

$$s^{(m)}[i] = \int_{-\infty}^{+\infty} f(x)\phi^{(m)}(x - 2^m i)dx \qquad (11)$$

and $\phi^{(m)}(x)$ is the dilated version of $\phi^{(0)}$, which is given by

$$\phi^{(m)}(x) = 2^{-m/2}\phi^{(0)}\left(\frac{x}{2^m}\right). \qquad (12)$$

Consider the basis function at scale $(m + 1)$, which is completely embedded in scale (m). Mallat (1989a,b) showed how the coarse-grained version $s^{(m+1)}[i]$ can be obtained from $s^{(m)}[j]$ using the convolution

$$s^{(m+1)}[i] = \sum_{j=-\infty}^{j=+\infty} h[j - 2i]s^{(m)}[j], \qquad (13)$$

where $h[u]$ is defined by

$$h[u] = 2^{-1/2} \int_{-\infty}^{+\infty} \phi^0 \frac{y}{2} \phi^0(y - u)dy. \qquad (14)$$

Similarly, the wavelet coefficients at scale $(m + 1)$ can be obtained from $s^{(m)}$ by

$$W^{(m+1)}[i] = \sum_{j=-\infty}^{j=+\infty} g[j - 2i]s^{(m)}[j], \qquad (15)$$

where $g[u]$ is defined by

$$g[u] = 2^{-1/2} \int_{-\infty}^{+\infty} \psi^0\left(\frac{y}{2}\right) \phi^0(y - u)dy, \qquad (16)$$

which corresponds to the wavelet function $\psi(x)$ dilated by a factor of 2 and sampled by the smoothing function $\phi(x)$. The filters $h(u)$ and $g(u)$ are called the quadrature mirror filter (QMF) and have been used in connection with filter banks (Rioul and Duhamel 1992; Basseville et al. 1992). Notice that in Eqs. (15) and (17), the coarse-grained version and the wavelet coefficients at a certain scale can be computed from the preceding scale. Figure 1 illustrates Mallat's (1989a,b) multiresolution algorithm for obtaining the wavelet coefficients and the coarse-grained series. Note in Fig. 1 that $h(u)$ acts as a low-pass filter that smooths the original series. The information lost in the smoothing is conserved by the bandpass filter $g(u)$, which conserves the difference in signal information between two consecutive octave scales. Another smoothing operation is then applied to the low-pass filtered signal, and the difference in information between the current scale and the next larger scale is conserved by the band-pass filter again (through the wavelet coefficients). This pyramidal scheme ends when the signal becomes a constant line and the low-pass filter yields a zero coefficient. In appendix A, a modification to the algorithm of Fig. 1 is presented to yield a fast algorithm (order N) that computes the Haar wavelet coefficients as well as the coarse-grained version of the signal at various scales. Appendix B presents some of the important properties of these orthonormal wavelets.

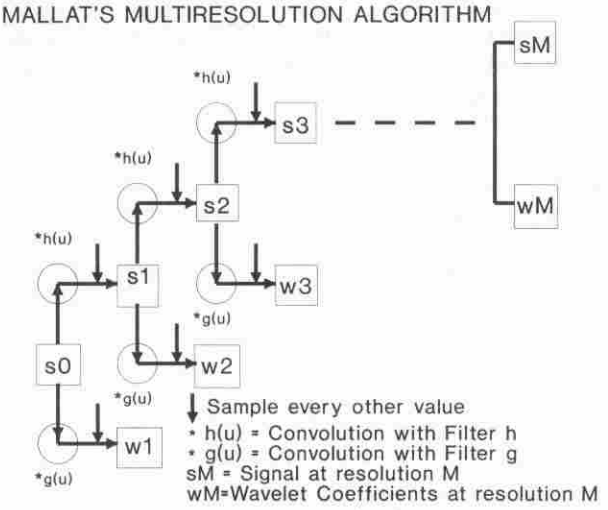

FIG. 1. Mallat's multiresolution pyramidal algorithm to obtain the coarse-grained signal $s(\ )$ and the wavelet transformed signal $w(\ )$ at different scales. The coarse-grained signal is obtained by a convolution with the $h(\ )$ filter, which is analogous to a low-pass filter, while the wavelet transformed signal is obtained by a convolution with the $g(\ )$ filter, which is the discrete version of the continuous wavelet.

b. Wavelet statistics of turbulence

One of the primary tools in the characterization of turbulence is the power spectral density function $E(k)$ that represents the energy density contained in the wavenumber bandwidth dk (Tennekes and Lumley 1972; Monin and Yaglom 1975). Because of the global nature of this transform, all information related to position is lost. In this section, the wavelet dual spectrum as well as other statistical measures are presented that allow information regarding position to be preserved.

1) WAVELET SPECTRA

For normalization purposes and for comparisons with Fourier transforms, the time average is subtracted from the original signal so that each signal has a zero mean value. In addition, it is assumed that the observations are sampled every (dy) meters instead of at unit length. The variance of the signal, in terms of the wavelet coefficients, is deduced from (6) using

$$\sigma^2 = N^{-1} \sum_{m=1}^{m=M} \sum_{i=1}^{i=N} (W^{(m)}[i])^2, \qquad (17)$$

where N is the number of observations (multiples of 2), M is $\log_2(N)$, m is the scale index, and i is the position index. The total energy T_E contained in scale $R_m = (2^m dy)$ is given by

$$T_E = N^{-1} \sum_{i=1}^{i=2^{M-m}} (W^{(m)}[i])^2. \qquad (18)$$

The wavenumber corresponding to scale R_m is

$$k_m = \frac{2\pi}{R_m}. \qquad (19)$$

The power spectral density function is (18) divided by the change in wavenumber (Δk_m), which is equal to $(2\pi)2^{-m}(dy)^{-1} \ln(2)$, or

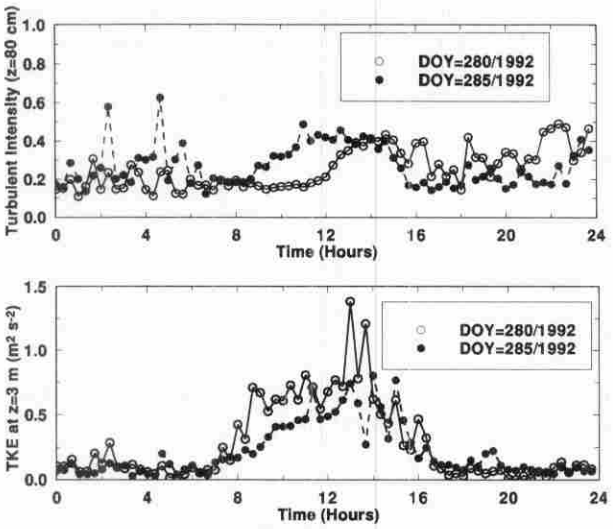

FIG. 2. The evolution of the turbulent intensity at 80 cm and the turbulent kinetic energy (TKE) at 3 m during the Julian days 280 and 285 of 1992.

$$E(k_m) = \langle (W^{(m)}[i])^2 \rangle \frac{dy}{2\pi \ln(2)}, \qquad (20)$$

where $\langle \cdot \rangle$ is the averaging in space over all values of i (see Meneveau 1991a). The standard deviation about this spatially averaged energy at k_m can also be computed from the wavelet coefficients using

$$\mathrm{SD}_E(k_m) = \frac{dy}{2\pi \ln(2)} [\langle (W^{(m)}[i])^4 \rangle - \langle (W^{(m)}[i])^2) \rangle^2]^{1/2}. \qquad (21)$$

Following Meneveau (1991a,b), a plot of $E(k_m)$ and $E(k_m) + \mathrm{SD}_E(k_m)$ gives a compact representation of the energy and its spatial variability at each scale, referred to as the "dual spectrum."

2) WAVELET SKEWNESS AND FLATNESS FACTORS

In addition to the standard deviation, one can compute the skewness $\mathrm{SF}(k_m)$ and the flatness factors $\mathrm{FF}(k_m)$ of the spatial distribution of the energy at each scale using

$$\mathrm{SF}(k_m) = \frac{\langle (W^{(m)}[i])^3 \rangle}{\langle (W^{(m)}[i])^2 \rangle^{3/2}}, \qquad (22)$$

$$\mathrm{FF}(k_m) = \frac{\langle (W^{(m)}[i])^4 \rangle}{\langle (W^{(m)}[i])^2 \rangle^{4/2}}. \qquad (23)$$

3. Experimental setup

Experiments were carried out at the University of California, Davis, Campbell Tract Research Facility. The site is a 500 m × 500 m uniform bare soil field with an average momentum roughness height (z_0) of 2 mm (Katul and Parlange 1992). A Campbell Scientific one-dimensional sonic anemometer, a krypton hygrometer, and a fine-wire thermocouple were installed at 80 cm above the ground surface. Measurements of water vapor density fluctuations were made with the krypton hygrometer (pathlength = 1.105 cm) while temperature fluctuations were measured with a 0.0127-mm chromel constantan thermocouple. Two 1-hour sets of measurements with a sampling frequency of 10 Hz were carried out using the krypton hygrometer and the fine-wire thermocouple. The first experiment was carried out on day of year 280/1992 at 1:32 P.M., and the second experiment was carried out on day of year 285/1992 at 10:39 P.M. The wind speed at 80 cm was sampled every 1 second with a 3-cup photochopper anemometer (sensitivity = ± 0.2 m s^{-1}) and averaged every 20 minutes. Figure 2 shows the 20-minute averaged turbulent intensity as well as the turbulent kinetic energy (TKE) throughout days 280 and 285. During the experiments the turbulent intensities were less than 0.5, and Taylor's hypothesis was used to convert time measurements to space measurements (e.g., Taylor 1938; Lumley 1965; Powell and Elderkin 1974; Willis and Deardorff 1976; Wyngaard and Clifford 1977). Table 1 summarizes some meteorological and turbulence statistics also measured in these two experiments.

4. Spectral properties of turbulence at small wavenumbers

As shown in (1), the spectrum of turbulence is dependent on two dimensionless groups, kz and z/L. In this study, $z = 0.8$ m, which is smaller than $|L|$, so

TABLE 1. Meteorological and turbulence statistics during the two experiments. The standard deviation (σ) for the temperature (T) and specific humidity (q), the friction velocity (u_*), and the sensible (H) and latent heat flux (LE) are also shown. The integral time scale (L_I) was computed from the area under the autocorrelation function up to the first zero crossing as discussed in Sirivat and Warhaft (1983).

Day/time (1992)	Variable	σ	L_I (s)	u_* (m s^{-1})	LE (W m^{-2})	H (W m^{-2})	L (m)
280/1332	T	1.201°C	2.0	0.16	35	173	−2.4
	q	0.151 g m^{-3}	1.66				
285/2139	T	0.105°C	3.72	0.064	−9	−5	+5.1
	q	0.123 g m^{-3}	1.77				

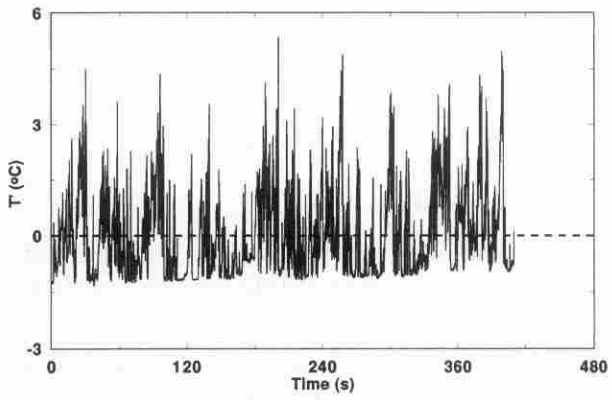

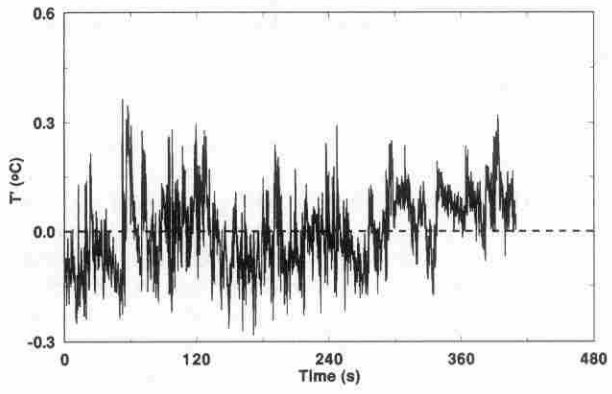

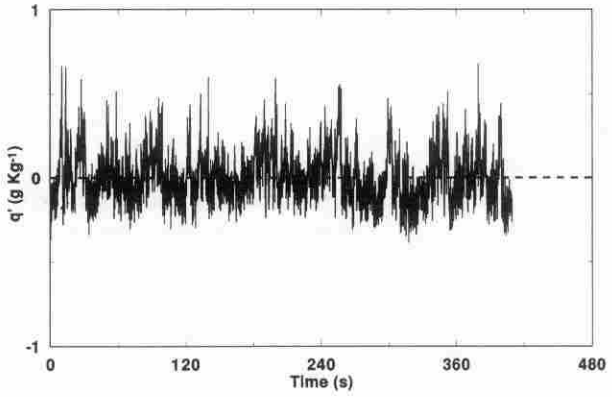

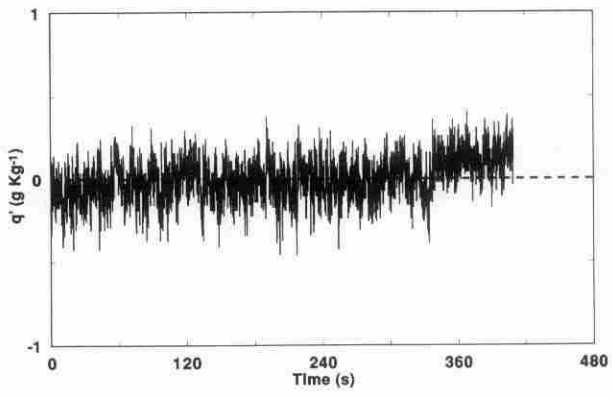

that z/L may not be as important as kz. Also, following Kader and Yaglom (1991), it seems reasonable to assume that the statistical regime of the large eddies close to the ground surface is independent of height z so that

$$\frac{E_i(k)}{zu_*^2} = \frac{C_i}{kz}$$

$$\frac{E_T(k)}{zT_*^2} = \frac{C_T}{kz}$$

$$\frac{E_q(k)}{zq_*^2} = \frac{C_q}{kz} \tag{24}$$

and the power spectra of velocity, temperature, and humidity fluctuations are given by

$$E_i(k) = C_i u_*^2 k^{-1}$$

$$E_T(k) = C_T T_*^2 k^{-1}$$

$$E_q(k) = C_q q_*^2 k^{-1}. \tag{25}$$

The -1 power law spectrum for small wavenumbers was originally derived for the longitudinal velocity by Perry and Abell (1975) in pipe flow, and for atmospheric flow by Kader and Yaglom (1991).

5. Results and discussion

Wavelet and Fourier analyses are applied to the temperature and specific humidity signals measured under unstable and stable atmospheric conditions. Figures 3a and 3b display the temperature variation, while Figs. 3c and 3d display the specific humidity fluctuations in time ($N = 4096$ points in all four signals). In this analysis, the classical Fourier spectra are discussed first and then the wavelet spectrum is considered. Comparisons between the Fourier and the wavelet spectra are carried out. Results on the statistical description of spatial intermittency are presented, and the influence of the basis function using various wavelets is discussed.

a. Fourier power spectra

For the temperature and specific humidity signals under unstable and stable conditions, the Fourier power spectrum is computed and presented in Figs. 4a, 4b, 4c, and 4d. Windowing every 1024 points, cosine tapering 5% at each edge, and then averaging were used to generate the power spectrum. The wavenumber was given by $2\pi/(NdtU)$, where dt is the sampling time ($=0.1$ s) and U is the 20-min mean horizontal wind speed. Since the mean horizontal wind speed for the stable and un-

FIG. 3. The measured temperature fluctuations at 80 cm above the ground surface for (a) Julian day 280 at 1332 (PST) and (b) Julian day 285 at 2139 (PST); (c) and (d) the specific humidity measurements on the respective days.

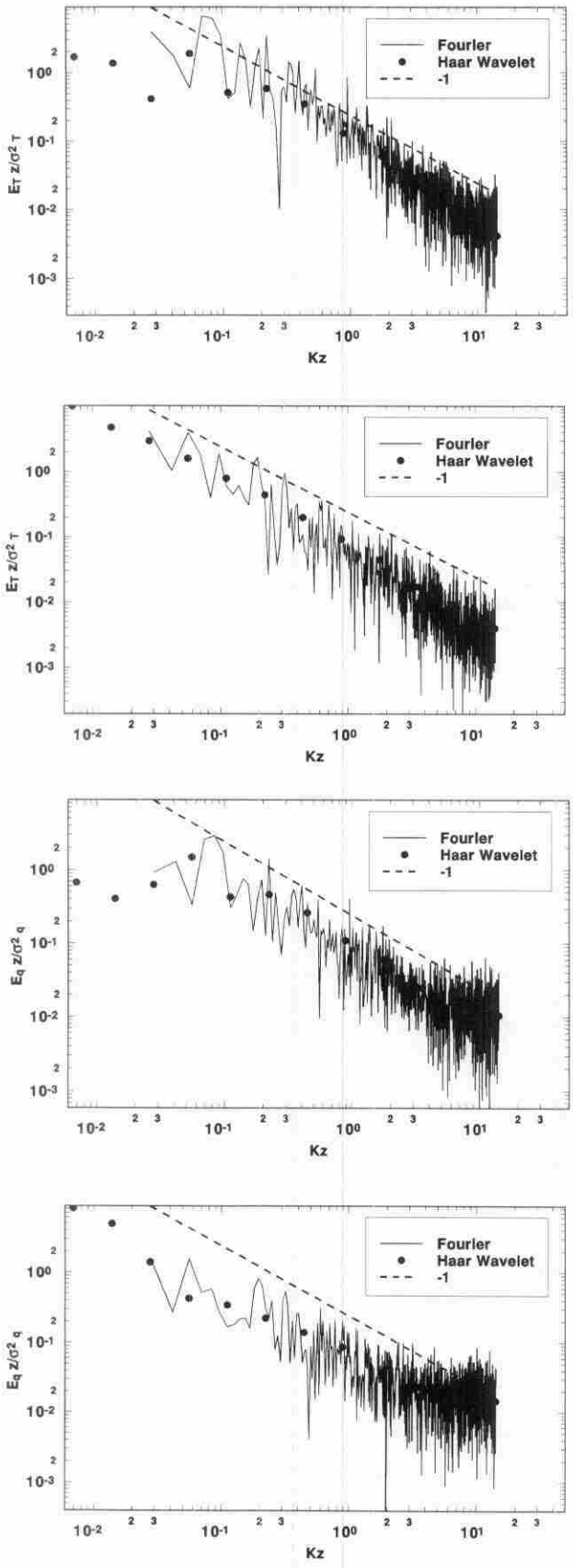

stable cases differed by only 0.1 m s^{-1}, an average value of $U = 1.7$ m s^{-1} was used for both stability conditions for the purpose of comparison. The existence of a -1 power law in which the energy density behaves as a power law function of wavenumber is observed for wavenumbers between 0.05 m^{-1} and 1 m^{-1} for the temperature signal under unstable conditions (see Fig. 4a). This production range is comparable to the wavenumber corresponding to the integral length scale = 1.85 m^{-1} (see Table 1). For stable stability (see Fig. 4b), the temperature signal exhibits a longer -1 production range (0.03 m^{-1}, 2 m^{-1}) that includes the wavenumber corresponding to the integral length scale (=0.994 m^{-1}; see Table 1). The spectral characteristics of the specific humidity fluctuations under unstable conditions (see Fig. 4c) are analogous to that of the temperature signal for the same stability (see Fig. 4a). The wavenumber corresponding to the integral length scale under unstable stability for the specific humidity signal is 2.23 m^{-1}, which is in agreement with the temperature wavenumber (1.85 m^{-1}) under unstable stability conditions (see Table 1). As for stable conditions (see Fig. 4d), a shorter specific humidity production spectrum with a -1 power law was noted (0.4 m^{-1}, 2 m^{-1}). The wavenumber corresponding to the integral length scale for the specific humidity under stable stability is 2.09 m^{-1} (see Table 1). The wavenumbers for these integral length scales were computed from the integral time scales of Table 1 using the method of Sirival and Warhaft (1983) and converted to length scales using Taylor's hypothesis

b. Multiresolution decomposition

The wavelet coefficients using the Haar (1910) basis function were computed for all four signals. For illustration purposes, the square of the wavelet coefficients for the temperature signal under stable conditions is shown in Fig. 5 as a function of space and scale. The sum of all these coefficients in space and scale is the variance of the measurements. Note how the number of coefficients increases and how the energy decreases as the scale decreases. The total energy content at each scale can be obtained by summing all the coefficients in space. These coefficients are also used to generate the wavelet power spectrum discussed next.

c. Wavelet spectra and comparison with Fourier spectrum

The Haar spectrum for the temperature and specific humidity measurements under unstable and stable con-

FIG. 4. A comparison between the Fourier (solid line) and the wavelet (open circles) power spectra for the temperature fluctuations collected on (a) Julian day 280 at 1332 and (b) Julian day 285 at 2139; (c) and (d) the specific humidity fluctuations on the respective days. The -1 power law is also shown.

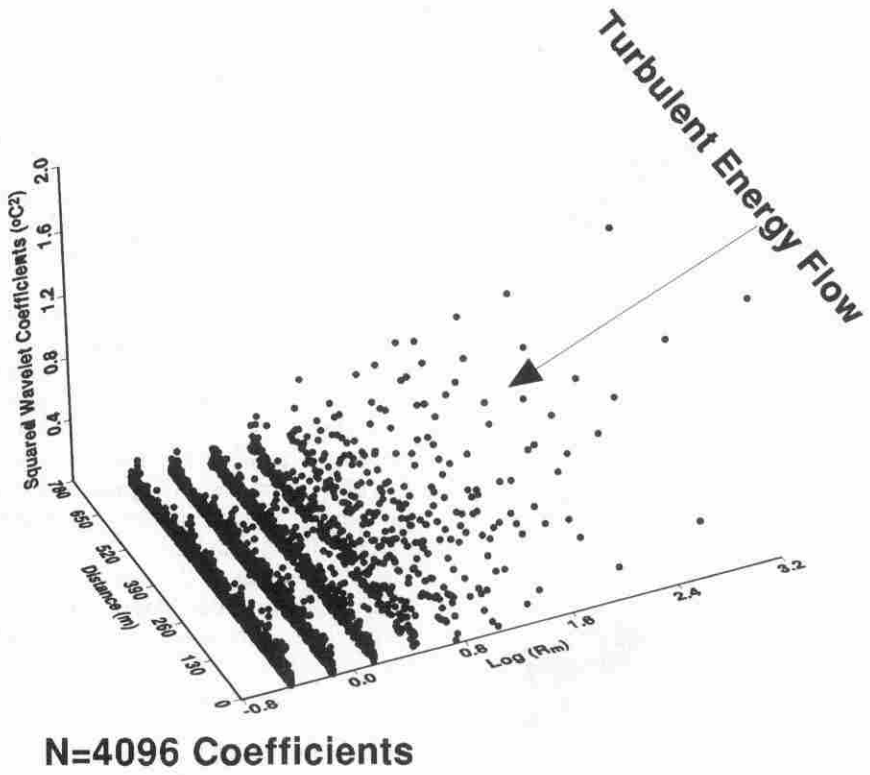

FIG. 5. The distribution of the square of the wavelet coefficients in space and scale for the Haar basis. The sum of the coefficients at all scales and positions yields the variance of the temperature measurements for Julian day 280 at 1332.

ditions is compared to the Fourier spectrum in Figs. 4a, 4b, 4c, and 4d. The two spectra agree; however, they are not identical since the Haar wavelet has finite locality in wave space (see appendix B). There is no unique turbulent spectrum per se since the signal is being decomposed into extended waves for the Fourier case and localized pulses for the Haar wavelet case (see Farge 1992a; Meneveau 1991a,b). Note the loss in scale resolution due to the dyadic arrangement of the wavelet spectrum in relation to the Fourier spectrum. The Haar wavelet spectrum appears to illustrate scaling laws better than the Fourier spectrum (see also Yamada and Ohkitani 1990; Benzi and Vergassola 1991). This is due to the fact that at each discrete scale, many wavelet coefficients are used to obtain the power content (see Fig. 5), and therefore, the wavelet spectrum is generally smoother than the Fourier spectrum. Note that in order to obtain a reliable estimate of the Fourier spectrum, the windowing and averaging procedures are necessary (see Shumway 1988, pp. 68–73; Press et al. 1990, pp. 420–429); therefore, the Fourier power spectrum does not extend to very small wavenumber

TABLE 2. Validation of the −1 Haar wavelet energy power law for temperature (T) and vapor (q) fluctuation. The range of wavenumber used to determine the slope is also shown. The regression statistics shown are for the model $\log[E(k_m)] = A \log(k_m) + B$. The coefficient of determination (R^2) and the standard error of estimate (SEE) are also displayed. The coefficient (C) for the production spectrum models $E_T = CT_*^2 k^{-1}$ and $E_q = Cq_{*2} k^{-1}$ are also shown.

Day/time (1992)	Variable	Wavenumber range (m^{-1})	R^2	SEE	Slope (A)	Intercept (B)	Coefficient (C)
280/1332	T	0.0723–2.31	0.93	0.154	−0.91	−0.58	0.41
	q	0.2888–2.31	0.99	0.04	−1.00	−2.43	0.49
285/2139	T	0.009–18.48	0.99	0.079	−1.03	−2.90	0.35
	q	0.018–0.0722	0.97	0.066	−0.95	−2.75	0.56

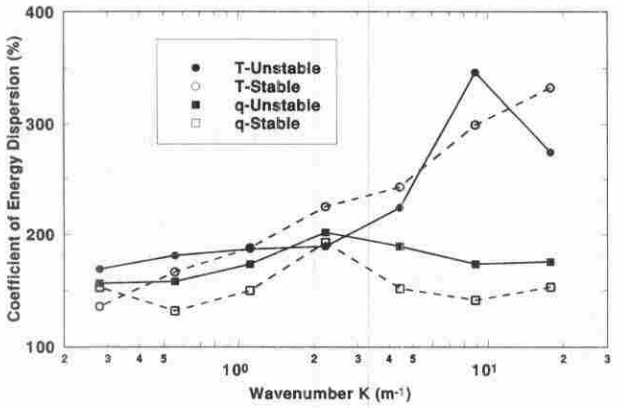

FIG. 6. The coefficient of energy dispersion at various wavenumbers for the temperature and specific humidity during both experiments using the Haar wavelet. Notice the similarity between the specific humidity and temperature at the large scales and the differences at the small scales.

when compared to the wavelet spectrum. The wavelet spectrum assigns the largest scale to the length of the record. For the Haar wavelet spectra, the -1 power law is clearly demonstrated (see Table 2) for the temperature and specific humidity measurements and for both stability conditions.

d. *Wavelet statistics*

As noted earlier, the wavelet decomposition permits the investigation of the spatial distribution of energy in space and scale. To study the distribution of energy in space, we modify Meneveau's (1991a,b) concept of dual spectra and propose a dimensionless energy dispersion measure given by

$$\mathrm{CV}(k_m) = \frac{\mathrm{SD}_E(k_m)}{E(k_m)}, \qquad (26)$$

where $\mathrm{CV}(k_m)$ is the coefficient of energy variation at wavenumber k_m. The coefficient of variation measures the contributions of local events to the energy dispersion at wavenumber k_m. Due to their nonlocal behavior, Fourier spectra assume that the energy is uniformly distributed in space at all wavenumbers [i.e., $\mathrm{CV}(k_m) = 0$]. A plot of the coefficient of variation as a function of k_m is shown in Fig. 6 for the temperature and specific humidity under unstable and stable stability. For the production wavenumbers (the -1 power law range), the energy dispersion is in excess of 100%, indicating that the variability of energy in space is large in relation to the mean value. Also, at smaller and smaller scales, the turbulent energy dispersion for the temperature fluctuations increases monotonically (see Fig. 6). This energy dispersion was not observed in the specific humidity measurements (see Fig. 6). At the small wavenumbers, which correspond to the -1 energy power law, the temperature and specific humidity measurements under unstable conditions appear to exhibit more energy dispersion when compared to the measurements obtained under stable conditions (see Fig. 6). However, the difference is not very large (at least for $k_m < 2$), which justifies the usual similarity assumptions between temperature and specific humidity as invoked by Monin and Obukhov (1954) surface-layer similarity theory. Also from Table 2, the coefficient C_T of the -1 production spectrum for temperature is nearly equal to that of C_q, indicating that both temperature and specific humidity act as passive tracers for the production wavenumber range. However, at larger wavenumbers ($k_m > 4$), the dissimilarity between temperature and specific humidity fluctuations becomes clear (see Fig. 6). It appears that the small-scale structure of temperature is more active (i.e., increased spatial variability in the turbulent energy) compared to the specific humidity. This is exposed more clearly by considering the Haar wavelet flatness factor shown in Fig. 7. Since the Haar wavelet is a localized jump in physical space, it amplifies events with the strongest spatial differences in the signal as opposed to the magnitude of events (see Mahrt 1991). Therefore, the Haar wavelet flatness factor measures the importance of the tails of the probability distribution of localized events (such as sharp edges) at wavenumber k_m. For the -1 energy power law range, near-Gaussian flatness factor statistics are computed (see Fig. 7). For large wavenumbers, however, the wavelet transformed temperature measurements are far from Gaussian, with flatness factors up to 15 (see Fig. 7). The wavelet-transformed specific humidity measurements, for both stability conditions, are nearly Gaussian at all wavenumbers, which is consistent with the coefficient of energy dispersion results of Fig. 6. Following Mahrt (1991), we use the wavelet skewness to measure the sign preference for strong horizontal gradients as well as their contribution to the overall anisotropy at that wavenumber. Figure 8 dis-

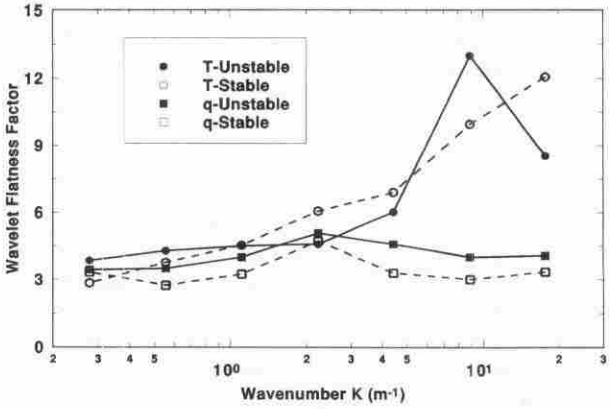

FIG. 7. Similar to Fig. 6 but for the Haar wavelet flatness factor. The flatness factor for a Gaussian distribution is 3.

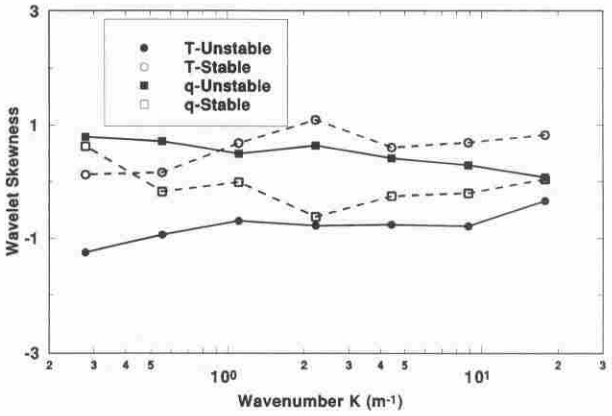

FIG. 8. Similar to Fig. 6 but for the Haar wavelet skewness.

plays the Haar wavelet skewness for the temperature and specific humidity as a function of wavenumber for both stability conditions. For stable stability, the anisotropy is negative at all production wavenumbers indicating that shear-induced asymmetry prevails, while for unstable stability the wavelet skewness is positive due to possible updraft–downdraft events (see Fig. 8). Also, marked differences between temperature and specific humidity statistics at large wavenumbers were measured. The specific humidity measurements, for both stability conditions, appear to attain a near-isotropic state (i.e., SF = 0) as the wavenumber increases (see Fig. 8). This near-isotropic state was not observed in the temperature signal, again pointing to the dynamically active role of temperature at small scales (see Fig. 8). We note that the temperature and specific humidity measurements were carried out at 80 cm over a dry bare soil field in which the heating or cooling at the ground surface is very inhomogeneous, and this nonhomogeneity can influence the turbulence transport of heat in the lower atmosphere. That the temperature statistics are similar to the specific humidity statistics at the larger scales, and the integral length scales of temperature and specific humidity are comparable, appears to indicate that close to the ground surface, temperature behaves like an active scalar at large wavenumbers compared to the specific humidity.

e. *Local characteristics of temperature fluctuations under stable atmospheric conditions*

It is assumed in (1) that the temperature behaves as a passive admixture that does not affect the dynamics of turbulence. It appears from the wavelet analysis that this assumption is reasonable since the spatial temperature statistics, at production wavenumbers and small $|z/L|$, resembles the specific humidity spatial statistics. Differences between temperature and vapor fluctuations appear at the large wavenumbers. This was investigated by Bolgiano (1959) for temperature fluctuations at large wavenumbers. Bolgiano (1959) generalized Kolmogorov's (1941) first hypothesis and assumed that for scales $l < L_l$, the temperature difference statistics can be uniquely determined from ϵ, N_T, g/T_a, ν, and χ, where ϵ is the dissipation rate, $N_T = \sigma_T^2/2$, σ is the standard deviation of the temperature fluctuations, ν is the viscosity of air, and χ is the thermal diffusivity. Analogous to the Obukhov length in the Monin–Obukhov surface-layer similarity theory (Monin and Obukhov 1954), Bolgiano (1959) proposed a length scale L_* given by

$$L_* = \frac{\langle \epsilon \rangle^{5/4}}{N_T^{3/4}(g/T_a)^{3/2}}. \tag{27}$$

This length scale measures the relative importance of the turbulence temperature dissipation relative to the turbulence temperature production. For stable atmospheric conditions, Bolgiano (1959) proposed that the energy transferred from disturbances of length $l \gg L_*$ to smaller disturbances should be much greater than $\langle \epsilon \rangle$, since most of this energy is used to overcome buoyancy, and only a small fraction of this energy cascades to the Kolmogorov microscale where it is dissipated. On this basis, Bolgiano argued that $\langle \epsilon \rangle$ will not influence the shape of the temperature spectrum in the region where $k \ll 1/L_*$. This led Bolgiano to propose an asymptotic form for the temperature spectrum for $k \ll 1/L_*$ since the temperature spectrum depends only on N_T and g/T_a, yielding

$$E_T = C_b N_T^{3/5} \left(\frac{g}{T_a}\right)^{-2/5} k^{-7/5}, \tag{28}$$

where C_b is a universal constant (see Monin and Yaglom 1975, p. 392). Monin and Yaglom (1975, p. 393) indicate that the applicability of Bolgiano's theory is restricted to heights larger than 100 m due to order of magnitude estimates that suggest L_* decreases as $z^{-1/2}$ while the external disturbances of length l increase as z. In this study, the temperature measurements were at 80 cm and the $L_l \sim 6$ m, so it is unlikely that Bolgiano's scaling law holds, at least for the range of wavenumbers measured, due to 1) the large anisotropy injected from the inhomogeneous cooling at the ground surface and 2) the continued production of turbulence at large wavenumbers (see Fig. 4b). If the influence of these inhomogeneities and production effects is suppressed by suppressing local events that are intermittent, energy containing, and anisotropic, then there could exist a wavenumber range in which Bolgiano's scaling law is obeyed. This hypothesis is tested using conditional wavelet spectra, which is discussed next.

f. *Conditional wavelet spectra and the recovery of Bolgiano's scaling law*

In order to suppress the anisotropic and energy containing eddies at a certain wavenumber k_m, we introduce the conditional wavelet spectrum defined by

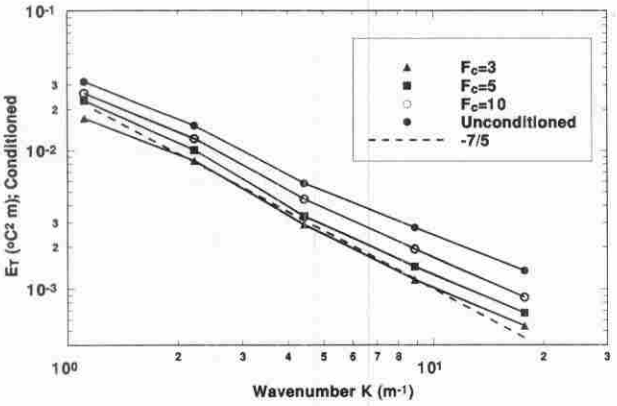

FIG. 9. The conditional Haar wavelet spectra for the three conditioning events. Notice how the spectrum approaches Bolgiano's scaling law (−7/5) as more and more energetic events are suppressed (i.e., F_c decreases).

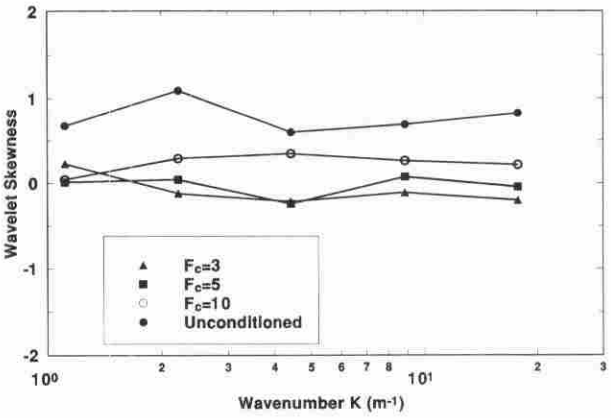

FIG. 10. A comparison between the conditioned and unconditioned wavelet skewness for the three conditioning events. Notice how the wavenumber range corresponding to Bolgiano's scaling law attains a near-isotropic state.

$$E(k_m) = \langle\langle (I_f W^{(m)}[i])^2 \rangle\rangle \frac{dy}{2\pi \ln(2)}, \qquad (29)$$

where $\langle\langle \cdot \rangle\rangle$ is the averaging over nonzero values and I_f is the indicator function defined by

$$I_f = \begin{cases} 1 & \text{if } \dfrac{W^m[i]^2}{\langle W^m[i]^2 \rangle} < F_c \\ 0 & \text{otherwise,} \end{cases} \qquad (30)$$

where F_c is some conditioning event. This conditional formulation eliminates the events that are F_c times larger than the mean value. Using the Haar wavelet, we computed the conditional wavelet spectrum for the temperature signal under stable conditions for F_c = 3, 5, and 10. Figure 9 shows the conditional wavelet spectra in relation to the −7/5 scaling law. Bolgiano's scaling law appears for nearly one full decade for F_c = 3 and 5 (see Table 3). In Table 3, the unconditioned decade yielded a slope of −1.23 which lies between the −1 (production scaling law) and Bolgiano's −1.4 scaling law. Therefore, the energy containing eddies appear to "contaminate" Bolgiano's scaling law within the wavenumber decade of Table 3. The conditional spectrum allowed us to suppress the influence of these eddies and obtain Bolgiano's scaling law. As discussed by Monin and Yaglom (1975), Bolgiano's theory also assumes that the turbulence achieves a locally isotropic state. In order to study whether local isotropy is attained within the decade in which Bolgiano's scaling law holds, we make use of the conditional skewness and flatness factors defined by

$$\mathrm{SF}_c(k_m) = \frac{\langle\langle (I_f W^{(m)}[i])^3 \rangle\rangle}{\langle\langle (I_f W^{(m)}[i])^2 \rangle\rangle^{3/2}}, \qquad (31)$$

$$\mathrm{FF}_c(k_m) = \frac{\langle\langle (I_f W^{(m)}[i])^4 \rangle\rangle}{\langle\langle (I_f W^{(m)}[i])^2 \rangle\rangle^{4/2}}. \qquad (32)$$

where $\langle\langle \cdot \rangle\rangle$ is again averaging over nonzero values and I_f is the indicator function. For local isotropy the wavelet skewness, which measures the sign preference of strong horizontal gradients at that wavenumber, should be zero. Figure 10 shows the wavelet skewness as function of wavenumber for the three conditional events F_c = 3, 5, and 10. Clearly the unconditioned signal is not locally isotropic (given the large SF). The two conditioned events (F_c = 3, 5) in which Bolgiano's scaling law was reproduced appear to exhibit zero wavelet skewness in space, indicating that local isotropy is attained (Fig. 10). Figure 11 indicates that near-Gaussian statistics, as measured by the conditioned wavelet flat-

TABLE 3. Conditional spectra for temperature measurements at 80 cm under stable stability conditions for various conditioning events (F_c). The regression model used to determine the scaling laws is $\log[E(k_m)] = A \log[k_m] + B$. The coefficient of variation (R^2) and the standard error of estimate (SEE) are also shown. The regression model was applied over the displayed wavenumber range.

F_c	Wavenumber range (m^{-1})	Slope A	Intercept B	R^2	SEE
3	2.31–9.24	−1.42	−5.18	0.999	0.021
5	2.31–9.24	−1.39	−1.39	0.994	0.039
10	2.31–9.24	−1.33	−5.11	0.994	0.046
(Unconditioned)	2.31–9.24	−1.23	−5.05	0.997	0.031

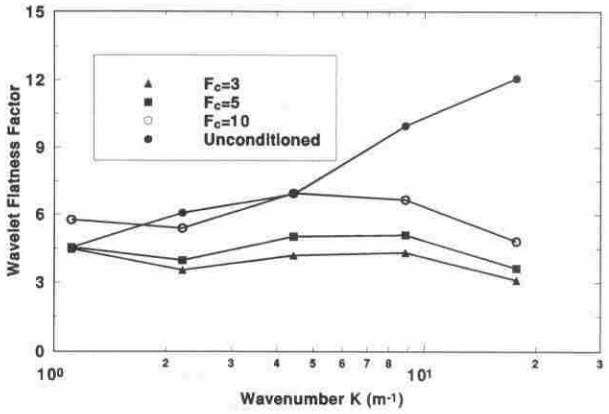

FIG. 11. Same as Fig. 10 but for the wavelet flatness factor.

ness factor, are associated with these two conditioning events. Note that the unconditioned event is much more intermittent, with wavelet flatness factors up to 12 (see Fig. 11). Note that for $F_c = 3$ the wavelet skewness and flatness factors (Figs. 10 and 11) are nearly identical to the unconditioned statistics of the specific humidity under stable stability conditions (Figs. 7 and 8). It is possible that the conditioning criteria (i.e., $F_c = 3$, 5) suppressed the influence of the ground temperature nonhomogeneity. This may explain the similarity between the conditioned temperature statistics and the unconditioned specific humidity wavelet statistics for stable atmospheric conditions.

g. *Influence of the basis function*

Unlike Fourier transforms, there is no unique basis function for the orthonormal wavelet transforms. Therefore, to assess the influence of the basis function on the spectral and statistical behavior of turbulence, we used the Daubechies wavelets with various vanishing moments (see Daubechies 1992, p. 195). The Daubechies wavelets are constructed so that the length of the wavelet is twice the number of vanishing moments in the wavelet. The wavelet spectra are compared in Fig. 12 for the temperature measurements under stable stability conditions. Except for the largest scale, all wavelets yielded identical spectral results. This indicates that the orthonormal wavelet spectrum is not very sensitive to the choice of the analyzing wavelet. For the sensitivity of the spatial statistics to the choice of the analyzing wavelet, we considered the wavelet flatness factor. Figure 13 compares the wavelet flatness factor for the temperature measurements under stable conditions. Note that even though the values do not compare as well as the spectra, the overall trend for all wavelets is essentially the same. The Haar wavelet appears to produce higher wavelet flatness factors compared to the Daubechies wavelets due to better localization in physical space.

6. Conclusions

Wavelet analysis is a useful way of quantifying atmospheric surface layer turbulence since "flow-independent eddies" are used in the decomposition of the

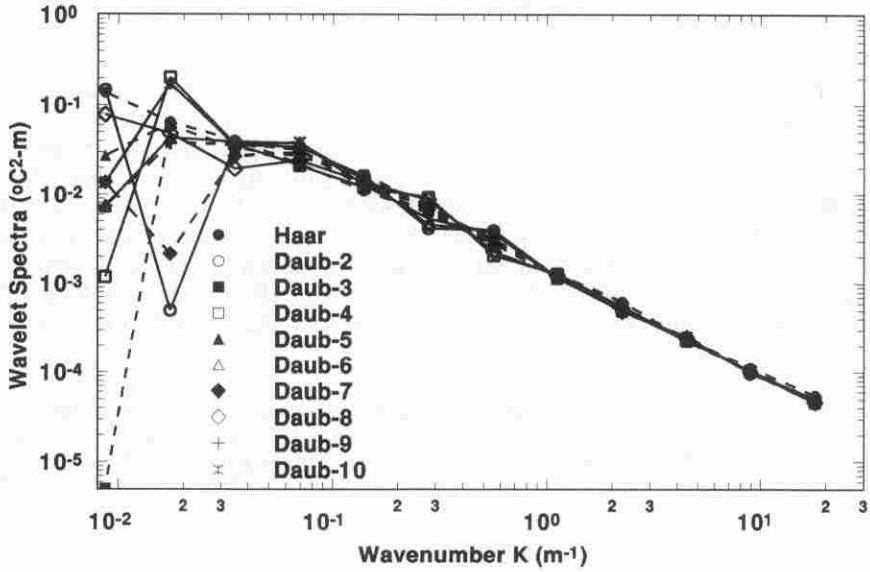

FIG. 12. The influence of the basis function on the spectral description of the temperature fluctuations for stable stability. The wavelets used are of the Daubechies type with various lengths and vanishing moments. For the Daubechies wavelet the filter length is twice the number of vanishing moments shown in the figure.

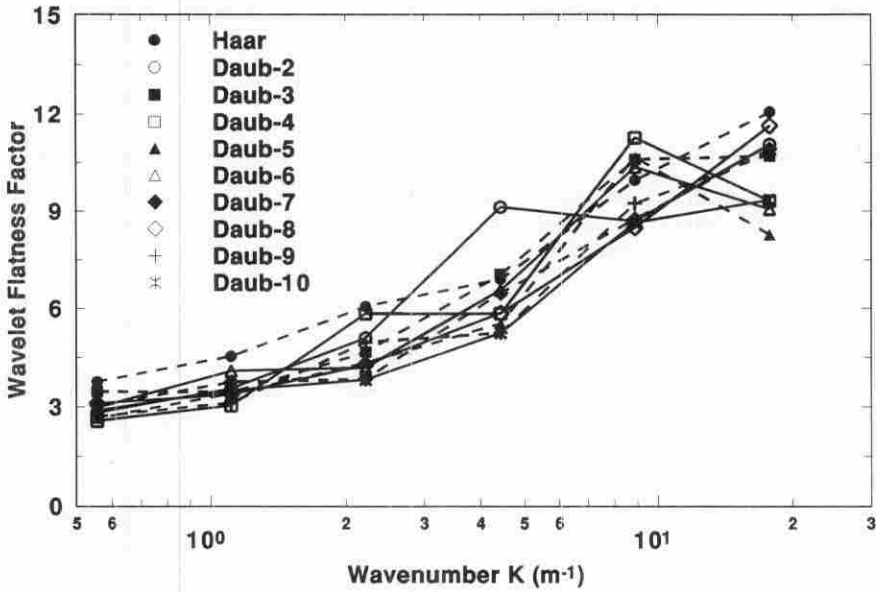

FIG. 13. Similar to Fig. 12 but for the wavelet flatness factor.

measurements. These transforms allow the decomposition of turbulent scalar fields such as temperature and humidity into space and scale, and information related to spatial statistics can be extracted. Wavelet spectra were computed and compared to the classical Fourier spectrum. It was shown that Fourier power spectra provide more scale information in relation to the orthonormal wavelet spectra; however, the wavelet spectrum appears to be smoother and capable of revealing energy scaling laws for atmospheric turbulence. At small wavenumbers, both the Fourier and Haar wavelet power spectra follow a -1 power law, consistent with measurements reported by Kader and Yaglom (1990). Simple dimensional argument, within the framework of surface-layer similarity theory for the large-scale eddies, demonstrated that such a scaling exists for near-neutral and height-independent conditions. The mean behavior of the wavelet spectrum matched the Fourier spectrum; however, large spatial fluctuations, as quantified by the coefficient variation about the mean values, were noted. Generally, due to the global nature of the Fourier transform, energy is distributed uniformly in space at all scales. For orthonormal wavelets, these nonuniformities in the energy distribution in space at various wavenumbers can be quantified. For that purpose, we introduced the coefficient of energy dispersion that measures how the energy is distributed in space at some wavenumber.

For the temperature fluctuations measurements, the energy dispersion around the mean value increased as the wavenumber increased indicating increased activity at the smaller scales. This was not observed in the specific humidity. The wavelet statistics for these scales indicate a similarity between the vapor and temperature, even though at the larger wavenumbers, a clear dissimilarity exists. The dissimilarity between vapor and temperature statistics at large wavenumbers is probably due to nonuniform heating and cooling at the ground surface that directly contributes to the active role of temperature in the dynamics of small-scale turbulence.

Conditional wavelet spectra were introduced and applied to the temperature measurements for stable stability conditions. Bolgiano's scaling law is obtained if conditional wavelet spectra are used with appropriate conditioning criteria. It was also shown that the wavelet skewness associated with the conditioned spectra had a value near zero, indicating that the conditioning criteria recovered the local isotropy structure.

The influence of the basis function on the spatial and spectral turbulence statistics was analyzed within the framework of the Daubechies wavelets. The turbulence power spectrum is not very sensitive to the choice of the analyzing wavelet. The wavelet statistics are more sensitive to the choice of the analyzing wavelet, namely, the fourth-order statistics. Nevertheless, the overall trend was the same for all ten wavelets considered.

Acknowledgments. The authors would like to thank Teresa Ortenburger and Mike Mata for their help in the data collection. The comments and suggestions of Roger Shaw and support from Dennis Rolston are gratefully acknowledged. This research has been supported and financed, in part, by the National Science Foundation (EAR-93-04331), State Salinity Drainage Task Force, Kearney Foundation, Water Resources

Center (W-812), USGS and the UC Davis superfund grant (5 P42ES04699-07).

APPENDIX A

Fast Wavelet Transform

In this appendix, a simple and fast algorithm to compute the Haar wavelet coefficients is reviewed. More details are found in Beylkin et al. (1991, 1992) and Zubair et al. (1992). The Haar basis with $h_{j,k}(x) = 2^{-j/2}h(2^{-j}x - k)$ with $j, k \in Z$, with

$$h(x) = \begin{cases} 1 & \text{for} \quad 0 < x < \frac{1}{2} \\ -1 & \text{for} \quad \frac{1}{2} \leq x < 1 \\ 0 & \text{elsewhere.} \end{cases} \tag{33}$$

The wavelet coefficients $W^{(j+1)}(k)$ and the coarse-grained signal $S^{(j+1)}(k)$ at scale $j + 1$ can be determined from the signal $S^{(j)}$ at scale j using

$$W^{(j+1)}(k) = \frac{1}{\sqrt{2}}[S^{(j)}(2k - 1) - S^{(j)}(2k)] \tag{34}$$

$$S^{(j+1)}(k) = \frac{1}{\sqrt{2}}[S^{(j)}(2k - 1) + S^{(j)}(2k)] \tag{35}$$

for $j = 0$ to $M - 1$, $k = 0$ to $2^{M-j-1} - 1$, and $M = \log_2(N)$; N is the number of samples. The above procedure, which is the basis for fast wavelet transforms, requires about N computations in comparison with the $N \log_2 N$ computations for fast Fourier transforms (FFT). Also, as can be noted from Fig. A1, this arrangement ensures orthonormality since the support of the smaller wavelet is completely embedded in the support of the larger wavelet.

APPENDIX B

Properties of Orthonormal Wavelets

The orthonormal wavelets used obey specific conditions:

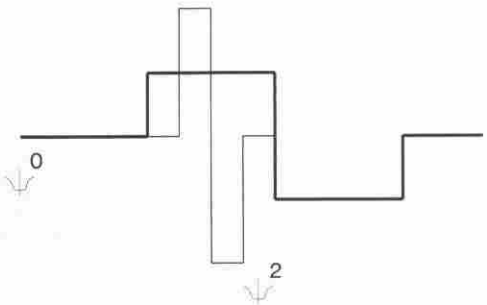

FIG. A1. Orthogonality of the Haar wavelet. Note how orthogonality ensures no overlap of wavelets at differents scales since the smaller wavelets are completely embedded in the larger wavelets.

1) All wavelet basis are orthonormal so that

$$\int_{-\infty}^{+\infty} \psi^{(m)}(x - 2^m i)\psi^{(n)}(x - 2^n j)dx = \delta_{ij}\delta_{mn}. \tag{36}$$

2) The wavelet basis are perpendicular to the smoothing or sampling function so that

$$\int_{-\infty}^{+\infty} \phi^{(m)}(x - 2^m i)\psi^{(m)}(x - 2^m j)dx = 0. \tag{37}$$

3) The smoothing or sampling function is orthonormal to itself at any scale m so that

$$\int_{-\infty}^{+\infty} \phi^{(m)}(x - 2^m i)\phi^{(m)}(x - 2^m j)dx = \delta_{ij}. \tag{38}$$

Note that condition (2) suppresses undesired relations between the sampling function and the mother wavelet. The Haar and the Daubechies wavelets all satisfy the above conditions; however, different wavelets have different localities in physical and Fourier domain. It should be noted that spatial localization and wavenumber localization are complementary (Zubair et al. 1992); that is, some loss of localization in one domain is required to improve the localization in the other domain.

REFERENCES

Argoul, F., A. Arneodo, G. Grasseau, Y. Gagne, E. J. Hopfinger, and U. Frisch, 1989: Wavelet analysis of turbulence reveals the multifractal nature of the Richardson cascade. *Nature,* **338,** 51–53.

Baseville, M., A. Benveniste, K. Chou, S. Golden, R. Nikoukhah, and A. Willsky, 1992: Modeling and estimation of multiresolution stochastic processes. *IEEE Transactions on Information Theory,* **38,** 766–781.

Benzi, R., and M. Vergassola, 1991: Optimal wavelet analysis and its application to two dimensional turbulence. *Fluid Dyn. Res.,* **8,** 117–126.

Berkooz, G., 1992: Observations on the proper orthogonal decomposition. *Studies in Turbulence,* T. Gatski, S. Sarkar, and C. Speziale, Eds. Springer-Verlag, 602 pp.

Beylkin, G., R. Coifman, and V. Rokhlin, 1991: Fast wavelet transforms and numerical algorithms I. *Comm. Pure Appl. Math.,* Vol. XLIV, 141–183.

——, ——, and ——, 1992: Wavelets in numerical analysis. *Wavelets and their Applications,* M. B. Ruskai, G. Beylkin, R. Coifman, I. Daubechies, S. Mallat, Y. Meyer, and L. Raphael, Eds. Jones and Bartlett, 474 pp.

Bolgiano, R., 1959: Turbulent spectra in a stably stratified atmosphere. *J. Geophys. Res.,* **67,** 3015–3023.

Chui, C. K., 1992: *An Introduction to Wavelets.* Academic Press, 264 pp.

Daubechies, I., 1988: Orthonormal bases of compactly supported wavelets. *Comm. Pure Appl. Math.,* Vol. XLI, 909–996.

——, 1992: Ten lectures on wavelets. *CBMS-NSF Regional Conference Series in Applied Mathematics, S.I.A.M.,* 61, 357 pp.

Everson, R., L. Sirovich, and K. R. Sreenivasan, 1990: Wavelet analysis of the turbulent jet. *Phys. Lett. A,* **145,** 314–322.

Farge, M., 1992a: Wavelet transforms and their applications to turbulence. *Annu. Rev. Fluid Mech.,* **24,** 395–457.

——, 1992b: The continuous wavelet transform of two dimensional turbulent flows. *Wavelets and their Applications,* M. B. Ruskai, G. Beylkin, R. Coifman, I. Daubechies, S. Mallat, Y. Meyer, and L. Raphael, Eds. Jones and Bartlett, 474 pp.

Grossmann, A., and J. Morlet, 1984: Decomposition of Hardy functions into square integrable wavelets of constant shape. *SIAM J. Math. Anal.*, **15,** 723–736.

——, and ——, 1985: Decomposition of functions into wavelets of constant shape, and related transforms. *Mathematics + Physics, Lectures on Recent Results,* Vol. 1, L. Streit, Ed. World Scientific, 338 pp.

——, R. Kronland-Martinet, and J. Morlet, 1989: Reading and understanding continuous wavelet transforms. *Wavelets: Time-Frequency Methods and Phase Space,* J. M. Combes, A. Grossmann, and Ph. Tchamitchian, Eds. Springer-Verlag, 315 pp.

Haar, A., 1910: Zur theorie der orthogonalen funktionensysteme. *Math. Ann.*, **69,** 331–371.

Kader, B. A., and A. M. Yaglom, 1990: Mean fields and fluctuation moments in unstably stratified turbulent boundary layer. *J. Fluid Mech.*, **1990,** 637–662.

——, and ——, 1991: Spectra and correlation functions of surface layer atmospheric turbulence in unstable thermal stratification. *Turbulence and Coherent Structures,* O. Metais, and M. Lesieur, Eds., Kluwer Academic, 387–412.

Katul, G. G., and M. B. Parlange, 1992: A Penman–Brutsaert model for wet surface evaporation. *Water Resour. Res.*, **28,** 121–126.

Kolmogorov, A. N., 1941: The local structure of turbulence in incompressible viscous fluid for very large Reynolds numbers. *Dokl. Akad. Nauk SSSR,* **4,** 299–303.

Kumar, P., and E. Foufoula-Georgiou, 1993: A new look at rainfall fluctuations and scaling properties of spatial rainfall using orthogonal wavelets. *J. Appl. Meteor.*, **32,** 209–222.

Liandrat, J., and F. Moret-Bailly, 1990: The wavelet transform: some applications to fluid mechanics and turbulence. *Eur. J. Mech., B/Fluids,* **9,** 1–19.

Lumley, J., 1965: Interpretation of time spectra measured in high intensity shear flows. *Phys. Fluids,* **6,** 1056–1062.

——, 1970: *Stochastic Tools in Turbulence.* Academic Press, 194 pp.

——, 1981: Coherent structures in turbulence. *Transition and Turbulence,* R. E. Meyer, Ed., New York Academic, 245 pp.

Mahrt, L., 1991: Eddy asymmetry in the shear heated boundary layer. *J. Atmos. Sci.*, **48,** 472–492.

Mallat, S., 1989a: A theory for multiresolution signal decomposition: The wavelet representation. *IEEE Trans. Pattern Analysis and Machine Intelligence,* **11,** 674–693.

——, 1989b: Multiresolution approximations and wavelet orthonormal bases of $L^2(R)$. *Trans. Amer. Math. Soc.*, **315,** 69–87.

Meneveau, C., 1991a: Analysis of turbulence in the orthonormal wavelet representation. *J. Fluid Mech.*, **232,** 469–520.

——, 1991b: Dual spectra and mixed energy cascade of turbulence in the wavelet representation. *Phys. Rev. Lett.*, **11,** 1450–1453.

Monin, A. S., and M. A. Obukhov, 1954: Basic laws of turbulent mixing in the ground layer of the atmosphere. *Tr. Geofiz. Instit. Akad. Nauk.* S.S.S.R., 163–187.

——, and A. M. Yaglom, 1975: *Statistical Fluid Mechanics.* Vol. II. J. Lumley, Ed. The MIT Press, 874 pp.

Perry, A. E., and S. J. Abell, 1975: Scaling laws for pipe-flow turbulence. *J. Fluid Mech.*, **67,** 257–271.

Powell, D., and C. E. Elderkin, 1974: An investigation of the application of Taylor's hypothesis to atmospheric boundary layer turbulence. *J. Atmos. Sci.*, **31,** 990–1002.

Press, W. H., B. P. Flannery, S. A. Teukolsky, and W. T. Vetterling, 1990: *Numerical Receipes: The Art of Scientific Computing.* Cambridge University Press, 702 pp.

Rioul, O., and P. Duhamel, 1992: Fast algorithms for discrete and continuous wavelet transforms. *IEEE Transactions on Information Theory,* **38,** 569–586.

Shumway, R. H., 1988: *Applied Statistical Time Series Analysis.* Prentice Hall, 380 pp.

Sirivat, A., and Z. Warhaft, 1983: The effect of a passive cross-stream temperature gradient on the evolution of temperature variance and heat flux in grid turbulence. *J. Fluid Mech.*, **128,** 323–346.

Taylor, G. I., 1938: The spectrum of turbulence. *Proc. Roy. Soc.*, A, Vol. CLXIV, 476–490.

Tennekes, H., and J. Lumley, 1972: *A First Course in Turbulence.* The MIT Press, 300 pp.

Willis, G. E., and J. Deordorff, 1976: On the use of Taylor's translation hypothesis for diffusion in the mixed layer. *Quart. J. Roy. Meteor. Soc.*, **102,** 817–822.

Wyngaard, J. C., and S. F. Clifford, 1977: Taylor's hypothesis and high-frequency turbulence spectra. *J. Atmos. Sci.*, **34,** 922–929.

Yamada, M., and K. Ohkitani, 1990: Orthonormal expansion and its application to turbulence. *Prog. Theor. Phys.: Progress Letters,* **86,** 819–823.

——, and ——, 1991a: Orthonormal wavelet analysis of turbulence. *Fluid Dyn. Res.*, **8,** 101–115.

——, and ——, 1991b: An identification of energy cascade in turbulence by orthonormal wavelet analysis. *Prog. Theor. Phys.*, **86,** 799–815.

Zubair, L., K. R. Sreenivasan, and M. V. Wickerhauser, 1992: Turbulent signals and images using wavelet-packets. *Studies in Turbulence,* T. Gatski, S. Sarkar, and C. Speziale, Eds. Springer-Verlag, 602 pp.